Geophys. J. Int. (2007) doi: 10.1111/j.1365-246X.2007.03435.x

Diana Wagner,[1] I. Koulakov,[2,3] W. Rabbel,[1] B.-G. Luehr,[2] A. Wittwer,[4] H. Kopp,[4] M. Bohm,[2] G. Asch[2] and the MERAMEX Scientists

[1]*Christian-Albrechts-Universität zu Kiel, Otto-Hahn Platz* 1, 24118 *Kiel, Germany. E-mail: diana@geophysik.uni-kiel.de*
[2]*GeoForschungsZentrum Potsdam, Telegrafenberg, Potsdam, Germany*
[3]*Institute of Geology, SB RAS, Novosibirsk, Russia*
[4]*IFM-GEOMAR, Kiel, Germany*

Accepted 2007 March 8. Received 2007 March 2; in original form 2006 June 30

SUMMARY

Seismic and volcanic activities in Central Java, Indonesia, the area of interest of this study, are directly or indirectly related to the subduction of the Indo-Australian plate. In the framework of the MERapi AMphibious EXperiments (MERAMEX), a network consisting of about 130 seismographic stations was installed onshore and offshore in Central Java and operated for more than 150 days. In addition, 3-D active seismic experiments were carried out offshore. In this paper, we present the results of processing combined active and passive seismic data, which contain traveltimes from 292 local earthquakes and additional airgun shots along three offshore profiles. The inversion was performed using the updated LOTOS-06 code that allows processing for active and passive source data. The joint inversion of the active and passive data set considerably improves the resolution of the upper crust, especially in the offshore area in comparison to only passive data. The inversion results are verified using a series of synthetic tests. The resulting images show an exceptionally strong low-velocity anomaly (−30 per cent) in the backarc crust northward of the active volcanoes. In the upper mantle beneath the volcanoes, we observe a low-velocity anomaly inclined towards the slab, which probably reflects the paths of fluids and partially melted materials in the mantle wedge. The crust in the forearc appears to be strongly heterogeneous. The onshore part consists of two high-velocity blocks separated by a narrow low-velocity anomaly, which can be interpreted as a weakened contact zone between two rigid crustal bodies. The recent Java $M_w = 6.3$ earthquake (2006/05/26-UTC) occurred at the lower edge of this zone. Its focal strike slip mechanism is consistent with the orientation of this contact.

Key words: Indonesia, joint inversion, subduction zone, Sunda Arc, tomography, volcanic structure

INTRODUCTION

Most of the damaging seismic and volcanic activity on the Earth is related to subduction zones. The recent destructive earthquake in Central Java (2006/05/26-UTC), which coincided with increased activity of Merapi volcano, is a dramatic illustration of close links between the subduction and surface tectonic activity. To understand the mechanisms which link the process of the sinking oceanic lithosphere to concurrent tectonic activity, seismicity and volcanism, it is important to obtain reliable information about the structure of the plate boundary volume involved: the shape of the slab, the 3-D structure of the crust and mantle wedge, and the distribution of seismicity. Seismic tomography is one of the most powerful tools to obtain these constraints.

In this study, we focus on the investigation of Central Java, a 200 km wide segment of the Sunda Arc, which extends from the Bay of Bengal and the Andaman Sea, along Sumatra and Java eastwards to Sumba Island (Fig. 1a). The deep-sea trench marks the boundary between the Indo-Australian plate and Eurasia where oceanic lithosphere is subducted beneath the Sunda Arc with a convergence rate of 6.7 ± 0.7 cm yr^{-1} in front of Java being approximately orthogonal to the trench (Tregoning *et al.* 1994; Fig. 1a). Along the Sunda Arc, the collision system and the subduction style change significantly. The collision system is oceanic–continental off Sumatra, transitional off Java and intraoceanic off Bali and Flores (Hamilton 1988). Kopp *et al.* (2005) determined that the subduction style is dominated by an accretionary regime along the western Sunda margin whereas along the Central Java margin an erosive regime exists. The subduction of oceanic basement relief including the RooRise, an oceanic plateau, causes a retreat of the Java deformation front between 109°E and 115°E northward by approximately 50–60 km from its normal curvature trend (Fig. 1b). Off Central Java a continuous accretionary wedge, an outer forearc high and forearc basin are not developed as recognized along the Sunda margin off

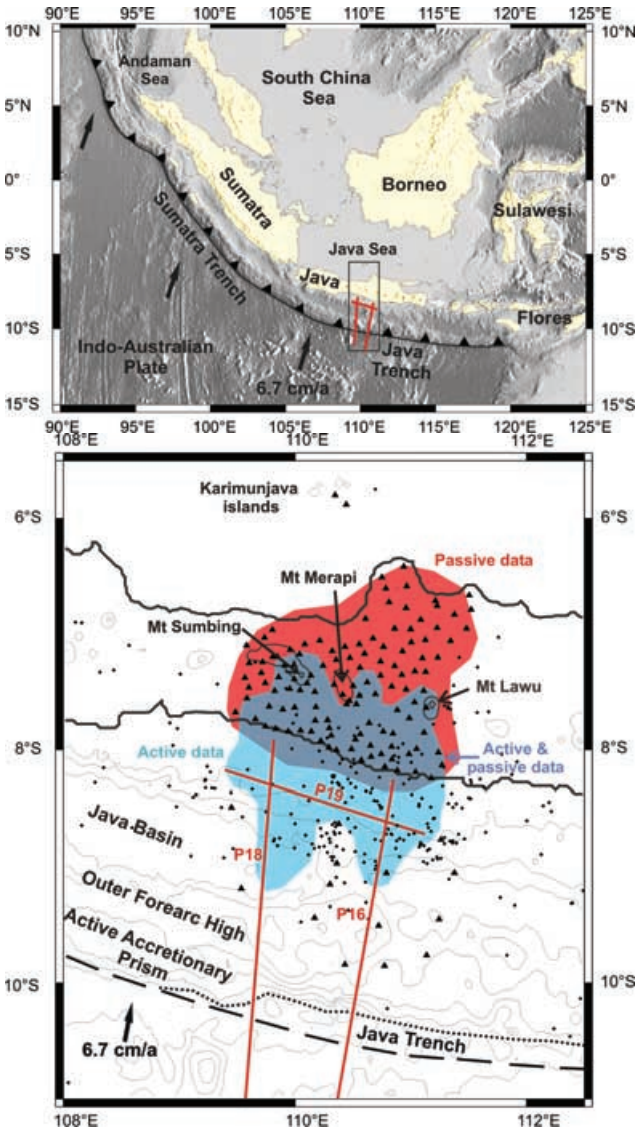

Figure 1. (a) Bathymetric map of the Sunda Arc. The Indo-Australian plate is subducted beneath the Eurasian plate along the Sumatra and Java trench. The location of our study area is marked by the box. (b) Study area including the tectonic regime of the region. The triangles mark the temporary seismological network. Dots are recorded earthquakes collected in the MERAMEX catalogue. Red lines indicate the seismic airgun profiles. The red coloured area in Central Java marks the area which is covered by the passive data, the light blue area is covered by active seismic data, while the grey area is covered by both data sets, respectively, in the uppermost 10 km depth layer. They are identified as areas with satisfactory recovery of 30 km size checkerboard anomalies at a depth of 5 km (Section Synthetic Tests, Fig. 6). The dotted line marks the current track of the trench, which is retreating northward from the normal curvature trend (dashed line) in front of Central Java.

Sumatra and West Java (Fig. 1b). Off western Java and southern Sumatra 96 Ma old oceanic crust subducts, while crustal ages increase to 135 Ma off eastern Java (Moore *et al.* 1980; Masson 1991). The subduction process along the active Sunda Arc is characterized by strong volcanism and high earthquake activity (Kennett & Cummins 2005; Mignan *et al.* 2006). More than 100 active volcanoes are located along the Sunda Arc, including Tambora and Krakatau. Their eruptions in 1815 and 1883 are known as two of the strongest and most destructive volcanic events in historical time.

The distribution of seismicity from the worldwide catalogue (ISC 2001) illustrates that off the south coast of Java, the dipping angle of the slab increases gradually from almost horizontal to very steep (70°–80°) north of Java. Beneath the Karimunjawa island group in the Java Sea, some moderate seismicity at a depth of around 600 km is observed.

Our study region includes Merapi volcano, which is the most active volcano in Java and represents a tremendous hazard to the local population. Mt Merapi is a strato volcano showing evidence of explosive eruptions over the last 7000 yr (Newhall *et al.* 2000). However, the volcanism at Mt Merapi began much earlier (Berthommier 1990; Camus *et al.* 2000). Most previous geophysical studies in Central Java focused on the internal structure of Mt Merapi (Maercklin *et al.* 2000; Wegler & Lühr 2001; Müller *et al.* 2002; Müller & Haak 2004). Seismological studies carried out by Ratdomopurbo & Poupinet (2000) show an aseismic zone situated between two seismic zones at a depth between 1.5 and 2.5 km below the summit. They postulate that this aseismic zone is caused by a small shallow magma reservoir temporarily storing injected magma from a deeper reservoir located below 5 km depth. Based on GPS and tilt data modelling, Beauducel & Cornet (1999) suggest a deep magma reservoir located some 6 km below sea level. The upper magma reservoir proposed by Ratdomopurbo & Poupinet (2000) could not be detected by Beauducel & Cornet (1999), but their results do not preclude the 'two reservoir' idea because the studies were carried out at different times. High resolution gravity modelling conducted by Tiede *et al.* (2005) shows high-density bodies beneath the volcanic summits of Mt Merapi, Mt Merbabu and Mt Telemoyo, which may be interpreted as magma reservoirs.

On 2006 May 26 at 22:54:01 UTC a strong magnitude $M_w = 6.3$ earthquake (source: NEIC & Harvard) occurred in Central Java, Indonesia about 25 km SSE of Yogyakarta (May 27 at 5:54 a.m. local time in Java, Indonesia) and caused more than 6000 fatalities. BGR (Federal Institute for Geosciences and Natural Resources) placed the hypocentre at a depth of 17 km, which implies that the earthquake occurred in the overriding Sunda plate well above the dipping Australian plate. Moment tensor solutions show a strike slip regime. However, it is not clear why this event displays a strike-slip mechanism, while the effect of the slab pushing should primarily cause compression in the forearc crust. Based on the results obtained in this study, we will propose an explanation for this fact.

In 2004, combined amphibious seismological investigations at 110°E were performed in the framework of the MERapi AMphibious EXperiment (MERAMEX) project to study a volcanic arc system as part of an active continental margin. More than 100 seismic stations operated continuously for more than 150 days (see details in the data section). The local seismicity data recorded at these stations were used to perform a local tomographic inversion (Koulakov *et al.* 2007). This study provided important information:

(1) The presence of a large low-velocity anomaly in the crust northward of the active volcanoes showing a high *Vp*/*Vs* ratio of 1.9.

(2) A low-velocity anomaly in the upper mantle, which is inclined towards the slab.

(3) The existence of a double seismic zone in the slab at 40–130 km depth with a dipping angle of about 45°.

(4) The shape of the slab in the Benioff zone, which is almost horizontal for the first 150 km away from the trench and then gradually increases to about 70° at 250 km depth.

Based on the results mentioned above, a mechanism of feeding the volcanoes in Central Java was proposed. Koulakov *et al.* (2007)

checked successfully the reliability of the most important features retrieved from the inversion of only passive data in the crust and upper mantle in a number of synthetic tests. In one test they defined a strong shallow anomaly (more than 30 per cent of amplitude and 0–5 km of depth interval) representing the Merapi-Lawu-anomaly (MLA), northward of the active volcanoes, to understand whether the observed low-velocity anomaly in the crust is an artefact due to some near-surface factors or whether it may be attributed to deep crustal structure. The results of this test showed that although the effect of downward smearing of a shallow anomaly is quite important, the images of the real data inversion cannot be obtained merely due to an effect of near surface anomalies. It shows that the crust in the MLA area consists of low-velocity material in all depth intervals, not only near the surface.

During the operation of the MERAMEX network, 3-D active seismic experiments were carried out offshore south of Central Java during RV Sonne cruise SO179. Airgun shots were fired along three profiles and recorded by ocean bottom stations. The seismic reflection and refraction data acquired along these profiles were forward modelled in two dimensions using a ray tracing method to obtain the deep structure of the main interfaces in the offshore part and the *P*-wave velocity field (Wittwer *et al.* 2007). Simultaneously, the signals from the airgun shots were recorded at onshore MERAMEX stations providing the unique opportunity to combine passive and active data for the same network. In this study, we update the passive data set used in Koulakov *et al.* (2007) with the active source data that gives us some important advantages compared to the previous study: for example, the enlargement of the resolution area (Fig. 1b) and the improvement of the model reliability and resolution because of significantly higher accuracy of the active data. One shortcoming of the passive data is that due to the trade-off between velocity and source locations, absolute velocities cannot be retrieved reliably. The active data yields constraints to fix the *P*-velocity distribution in the uppermost 20 km onshore and offshore. In particular, it was crucial for obtaining reliable crustal structure information around the recent Java earthquake (2006 May 26) to provide an explanation of its mechanism.

THE DATA SET

In May 2004, a temporary seismological network was installed in a dense grid of about 10–20 km station spacing around Merapi volcano in Central Java to monitor the natural seismic activity. The network consisted of 106 continuously recording short-period three-component seismometers (Mark L4–3D) in combination with Earth data loggers (EDL) and 14 broad-band stations operated with Guralp seismometers (CMG3T and CMG3ESP) and SAM data loggers. The sampling rate of the data loggers was 100 Hz. Nine ocean bottom hydrophones (OBH) and five ocean bottom seismometers (OBS) extended the land network offshore (Fig. 1). The offshore stations were in operation for a period of 18 weeks while the onshore network operated for 21 weeks.

In 2004 September/October RV Sonne set out to acquire seismic refraction and reflection profiles including mini-streamer, bathymetric, gravimetric and magnetic data. Three seismic profiles, the two dip lines P16 and P18 reaching from close to the coast across the trench onto the oceanic plate as well as profile P19 located about 25 km off the south coast of Java, were recorded both offshore on ocean bottom hydrophone (OBH) stations along the seismic profiles and onshore within the temporary seismological network (Fig. 1b). The seismic profiles were shot with an array of three 32-l (2000 inch^3) BOLT airguns (Model 800 CT Bolt), at a shot interval of 60 s and at a speed of approximately 4.9 knots (Fig. 2a and b). The land receivers stored the raw data of profiles SO179-P16, P18 and P19 in MiniSEED data format, which subsequently was converted to SEGY and sorted to receiver gathers. Spectral analyses of each receiver gather helped to determine the ideal filter section. The first arrival traveltimes were picked after applying a bandpass butterworth filter with filter corners of 3–12 Hz, a notch filter dependent on the individual receiver gather to eliminate spikes and a linear

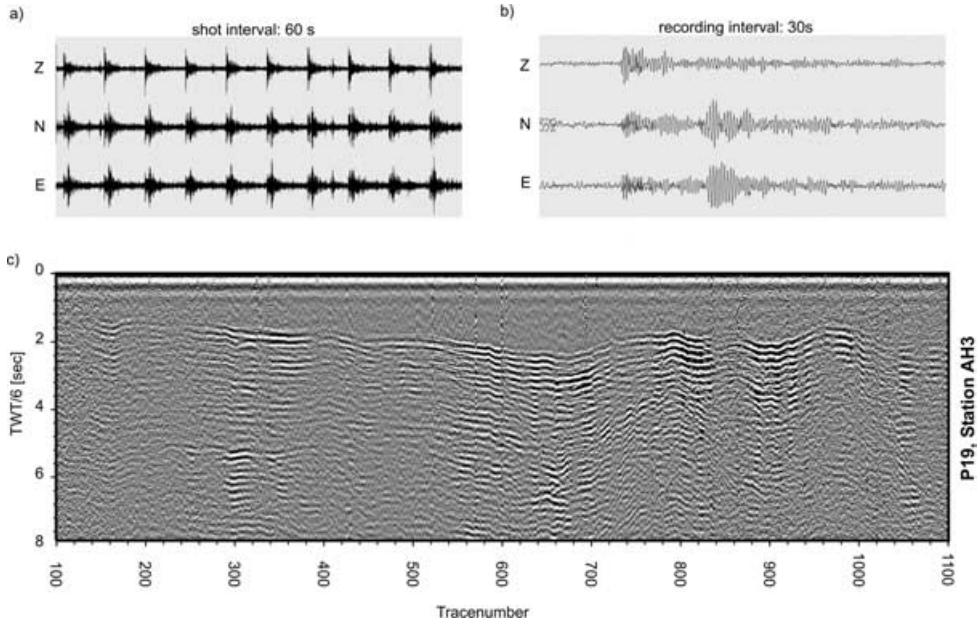

Figure 2. (a) Z, N and E components of airgun signals having a shot interval of 60 s recorded onshore. (b) Zoomed-in seismogram of one single airgun shot. The shown recording interval is 30 s. (c) Example of a seismic section of an onshore station (AH3) located southwest of Merapi volcano in Central Java. It shows the good data quality of the airgun profile P19 recorded onshore. The first onset of each trace of the coast-parallel profile can be picked at this onshore station.

moveout (reducing velocity) of 6 km s^{-1} to the raw data. Picking was facilitated by the small trace spacing of about 150 m, which provided excellent correlation between traces. A principal difficulty was the correct identification of first arrivals across an entire section. All traces were individually normalized. Fig. 2(c) shows a seismic section of station AH3, located in the south west of Mt Merapi. The section shows the receiver gather of the airgun shots of the coast parallel profile P19. The picking accuracy of the first arrivals was high, typically about 100 ms. Maximum offsets of about 150 km between shots and onshore receivers were common. The 3-D active seismic data consist of the shot data recorded within the onshore array. Airgun signals of profile P16 could be picked at 26, of profile P18 at 28 and of profile P19 at 32 land receivers, resulting in 50060 picks. These receivers cover southern Central Java up to the volcanic arc (Fig. 1b). The passive data comprise the information from the 292 clearest local events detected during the operational period of the network. In total, 13 800 phases (8000 *P*- and 5800 *S*-phases) were handpicked and used for the simultaneous location of sources and tomographic inversion.

THE ALGORITHM

The data processing is performed using an updated version of code LOTOS-06 (Local Tomographic Software), which is described in detail in Koulakov *et al.* (2007) and allows processing for active and passive seismic data simultaneously. The reference 1-D model (Table 1) was parametrized by points at fixed depths and interpolated linearly in between. Down to a depth of 20 km, the *P*-velocity distribution was estimated based on the forward modelling results of the OBH data acquired within the MERAMEX project (Wittwer *et al.* 2007). For deeper parts, the *P*-velocity distribution was defined based on the global AK135 model (Kennett *et al.* 1995). For the *S*-velocity distribution, a-priori information was not at hand and was determined using a fixed *Vp*/*Vs* ratio of 1.78, which provided the minimum rms values after the first location step. Although this ratio is important for the source location, it has no significant effect on the relative velocity variations in the tomographic inversion, as shown in Koulakov *et al.* (2006b, 2007).

The iterative inversion algorithm consists of the following steps:

Step 1. Computation of the reference traveltime table. Approximate locations of natural sources in a 1-D velocity model are determined using a 3-D grid searching algorithm, based on the determination of an absolute extreme of a goal function (Koulakov & Sobolev 2006b). The extreme of the goal function is determined by searching the station with the minimum residual.

Step 2. In case of passive data the coordinates and traveltimes and in case of active data only the traveltimes are corrected according to a location algorithm, which maximizes the goal function following the direction of maximum gradient, similar to Koulakov *et al.* (2006a). This algorithm is designed for an arbitrary 3-D model and is based on the bending method of ray tracing (Um & Thurber 1987).

Table 1. 1-D velocity model.

Depth (km)	*Vp* (km s^{-1})
−3	4.3
3	4.9
8	5.7
16	6.9
24	7.1

Step 3. A parametrization grid is defined according to ray density. The nodes are placed in vertical planes spaced at 10 km from each other. The ray density defines the distribution of the nodes in each vertical plane and hence, in areas containing a small amount of rays, the distance between nodes is larger. The minimum spacing between nodes is fixed at 5 km to prevent extreme node concentrations in areas of high ray density. Due to effects and artefacts caused by a predefined grid orientation, the inversion is conducted in four differently oriented grids (0°, 45°, 90° and 135°) and then stacked. The 3-D velocity anomalies are computed at nodes distributed in the study volume. The nodes are joined together into tetrahedral blocks. Between nodes inside the tetrahedrons, the velocity distribution is interpolated linearly. The resolution of the model is controlled by smoothing and regularization parameters.

Step 4. The matrix construction is based on the computed ray paths. The residuals representing the effect of velocity variation in each node on the traveltime of each ray ($\partial t/\partial V$) are computed by integration along the ray paths (Koulakov *et al.* 2007). For the passive data, the matrix also includes the elements for source parameter corrections. To control the smoothing of the 3-D velocity models, a specific matrix block is added to the calculated matrix. Each line in this block contains two non-zero elements with opposite signs, corresponding to neighbouring parametrization nodes in the model. The corresponding data vector for this block is zero. Increasing weight of these elements have a smoothing effect upon the resulting anomalies. In this study, the estimation of the parameters for the inversion (smoothing, regularization and number of iterations) are based on results of synthetic tests with realistic anomalies and noise levels (Section 'Synthetic tests').

Step 5. The matrix inversion using a LSQR method is performed simultaneously for *P*- and *S*-velocity values, parameters of natural sources (four parameters for each source) and *P*- and *S*-station corrections (Koulakov *et al.* 2007). As a result, the velocity anomalies are computed on a 3-D irregular grid, which is subsequently interpolated to a regular grid. For the next iteration the velocity anomalies are added to the initial velocity model. Iterations are repeated until the contribution of the next cycle becomes negligible. In case of our study, five iterations were enough to achieve sufficient convergence.

RESULTS

Active data inversion

Active data picks amounted to a total of 50060. However, since the shot spacing was significantly smaller than the size of retrieved anomalies, it makes no sense to use the entire data set. In this case, the rays from close shots would produce almost identical equations, which would not improve the resolution of the tomographic model. Therefore, only one of two picks is used for the final inversion. We found that in the cases of the entire and reduced data sets, the inversion yielded very similar results. However, due to the lack of space, results of this comparison are not presented here.

The resulting distribution of *P*-velocity anomalies after the inversion of only active data is shown in Fig. 3 in horizontal sections (upper row). The rms values of the residuals in five iterations are presented in Table 2. The value in iteration 1 resulted from ray tracing in the 1-D starting model. Velocity perturbations are only shown if the distance to the nearest parametrization node is less than 10 km. Since the nodes were placed according to the ray density and distributed only in areas with sufficient ray coverage, results are only plotted in well-resolved parts of the investigated volume.

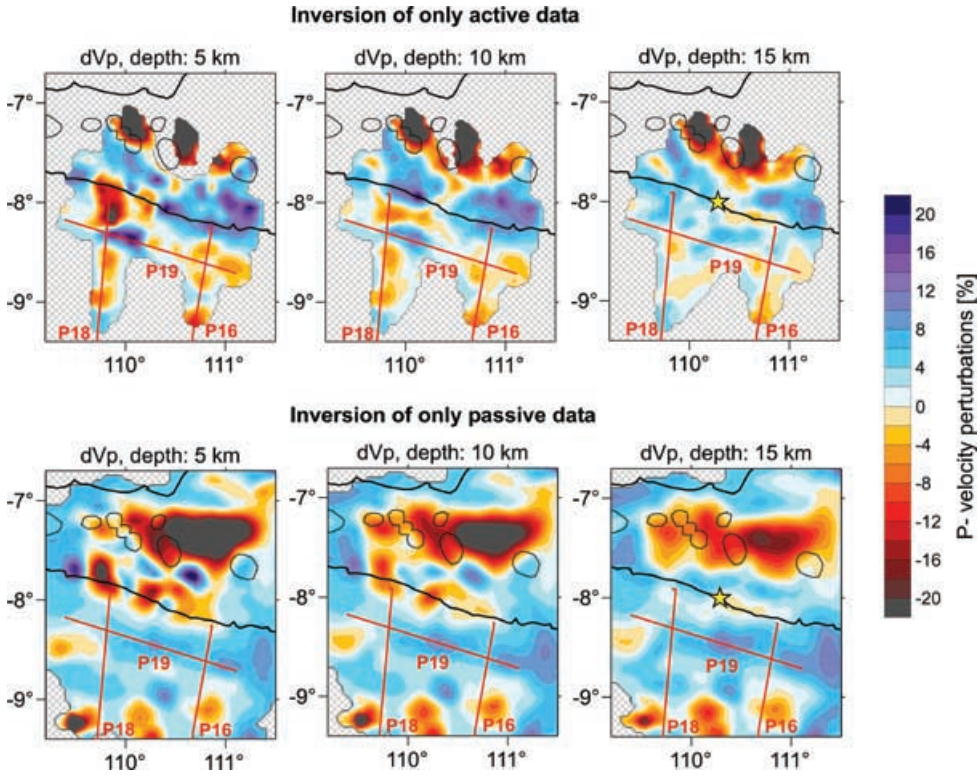

Figure 3. *P*-velocity anomalies after inversion of only active and only passive seismic data presented in horizontal sections at 5, 10 and 15 km depth. The black lines are the coastline and volcanoes located in Central Java. The airgun profiles are plotted with red lines.

Sumbing, Merapi and Lawu volcanoes are located above a very sharp boundary between a high-velocity forearc and a very strong negative anomaly northward of the volcanoes. This negative anomaly is called MLA. Although it occurs near the edge of the resolved area, this feature seems to be fairly robust. The forearc in these images appears to be strongly heterogeneous due to the complex geological structure of this area. South of Merapi, in the onshore part, an elongated zone of relatively low velocities is recognized. It is noteworthy that the hypocentre of the last strong earthquake event (2006 May 26), indicated by a yellow star in Fig. 3, is located exactly in this zone. In the offshore part, the dominant feature is a high-velocity pattern at the intersection of seismic profiles P18 and P19 resolved at 5 km depth. It extends to the east along the coast parallel to profile P19, as is also clearly visible in the seismic wide-angle forward models of these profiles (Wittwer *et al.* 2007).

Passive data inversion

The lower row in Fig. 3 shows the *P*-velocity perturbations obtained after the inversion of passive data (Koulakov *et al.* 2007). The most prominent feature is the strong low-velocity anomaly MLA, with over 30 per cent amplitude for the *P*-velocity in the crust. The volcanoes (Sumbing, Merapi and Lawu) are located just above the edge of the contact zone between the MLA and the highly heterogeneous forearc. The rms values of the residuals of the five inversion iterations are given in Table 3. It can be seen that the variance reduction after the final inversion is relatively small, about 35.4 per cent for *P* data. The remaining residuals could be caused by random noise in the data. Koulakov *et al.* (2007) performed a test in which the data set was divided and inverted independently, obtaining the same image which shows that random noise does not play a significant role. Therefore, the explanation of the residuals may be related to some real features not taken into account by our model. For example, it might be that strong small velocity patterns, which cannot be resolved by our model, still have an effect on traveltimes. In the zone of active volcanism, there could be relatively small magma pockets (up to 1 km) in the crust and uppermost mantle. Another explanation might be related to anisotropy, which can be quite important but is not taken into account in our study.

In general, the results obtained using independent passive and active data correlate fairly well (Fig. 3). The most prominent negative anomaly MLA just north of the volcanoes is clearly observable in both models. The shape of the interface between MLA

Table 2. The rms values of the residuals after five inversion iterations for only active data.

Iteration	Active, *P*, rms (s)
1	0.4047983
2	0.2229798
3	0.1697343
4	0.1509526
5	0.1404346

Table 3. The rms values of the residuals after five inversion iterations for the passive data.

Iteration	Passive, *P*, rms (s)	Passive, *S*, rms (s)
1	0.4464233	0.7856368
2	0.3447699	0.5819924
3	0.3133518	0.5314015
4	0.2977030	0.5073152
5	0.2883759	0.4923005

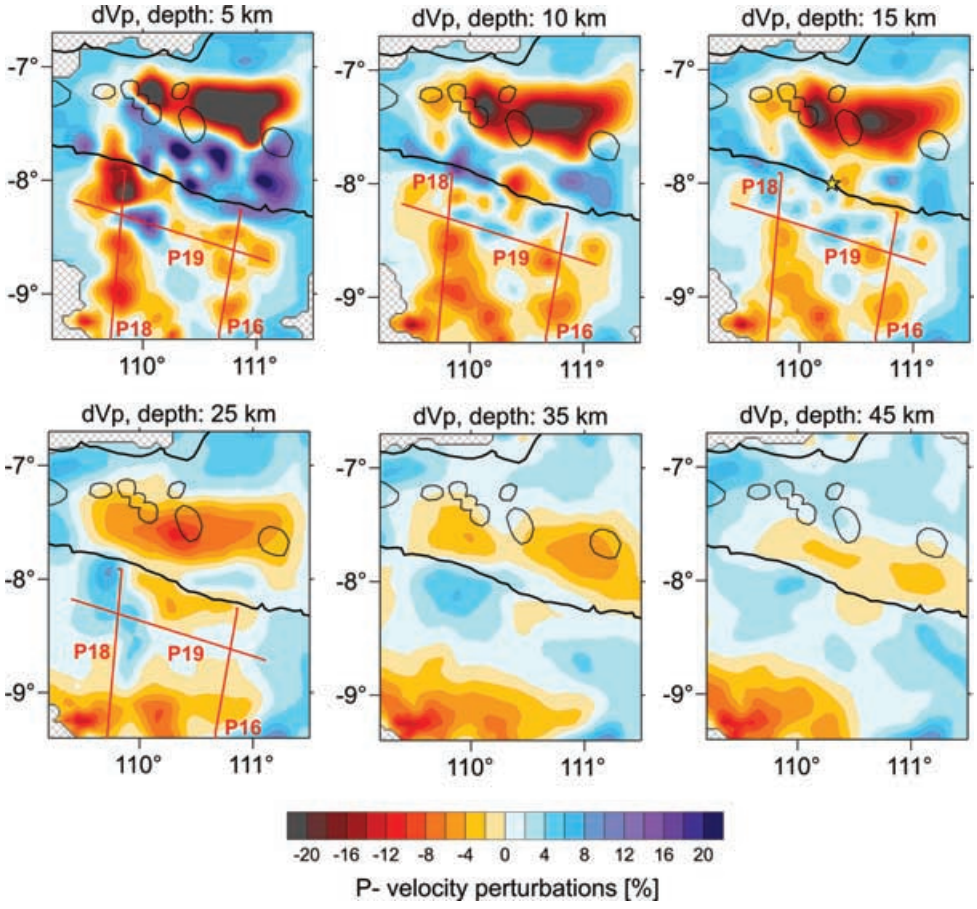

Figure 4. *P*-velocity anomalies after the joint inversion of the active and passive data sets presented in horizontal sections. Red lines indicate the airgun profiles. The star in the panel for 15 km represents the hypocentre location of the Java earthquake in 2006 May.

and the forearc is similar. In the uppermost parts of the forearc (5 and 10 km depth), the difference in velocity structures appears to be quite significant. It might be due to the different resolution of the passive and active seismic data sets. Shifting the colour scale achieves a better resemblance of the images. At a depth of 15 km, the images of both models are very similar.

Inversion of the combined active and passive data sets

The data used for the generation of the two models described in the previous sections were combined and inverted for a joint model. The weighting of corresponding rows in the general matrix controlled the contribution of the active data in the joint inversion. The same effect can be achieved by selecting a larger amount of active data, that is, more than 50 per cent. However, this approach requires more computer time. In summary, the *P*-velocity model in the horizontal sections as shown in Fig. 4 is essentially a mixture of active and passive models controlled by weighting of the active data set. In our case greater weight was given to the active data because they are less noisy and the offsets between source and receiver, as well as traveltimes of rays are well known compared to passive data.

It should be noted that although an inversion for *P* and *S* models with passive data was performed, only the *P*-velocity model is presented here. The rms values of the residuals are given in Table 4 separately for *P* rays in the active data, and *P* and *S* rays in the passive seismic data. The *S* model in this inversion remained almost unchanged both in images and rms values. Theoretically, *P* and *S* models are linked through source parameters, which are inverted simultaneously. However, in practice, the effect of *P*-velocity variation on the *S* model is fairly small. The distribution of earthquake hypocentres recorded in the MERAMEX network relocated after five iterations in the joint inversion model remained unchanged with respect to the solely passive inversion model (Koulakov *et al.* 2007).

Table 4. The rms values of the residuals after five iterations for the joint inversion. The rms values for active and passive *P*-velocities and passive *S*-velocities are shown.

Iteration	Active, *P*, rms (s)	Passive, *P*, rms (s)	Passive, *P*, rms (s)
1	0.4047983	0.4464233	0.7856368
2	0.2381959	0.3433573	0.5795938
3	0.1948432	0.3149615	0.5304253
4	0.1784572	0.3008182	0.5062090
5	0.1705896	0.2933580	0.4931750

The vertical sections in Fig. 5 show that the MLA extends into the upper mantle and is inclined towards the slab. The amplitude of the MLA changes from east to west as can be seen in the vertical sections (Fig. 5). Below Merapi and Lawu volcanoes (Profile 1 and 2, Fig. 5) the amplitude of the anomaly is much larger than beneath Sumbing volcano (Profile 3, Fig. 5). In the forearc, the crust shows inhomogeneous characteristics. Several low-velocity anomalies can be identified whose shapes are inclined towards the trench and coincide with the distribution of local seismicity. The correlation of

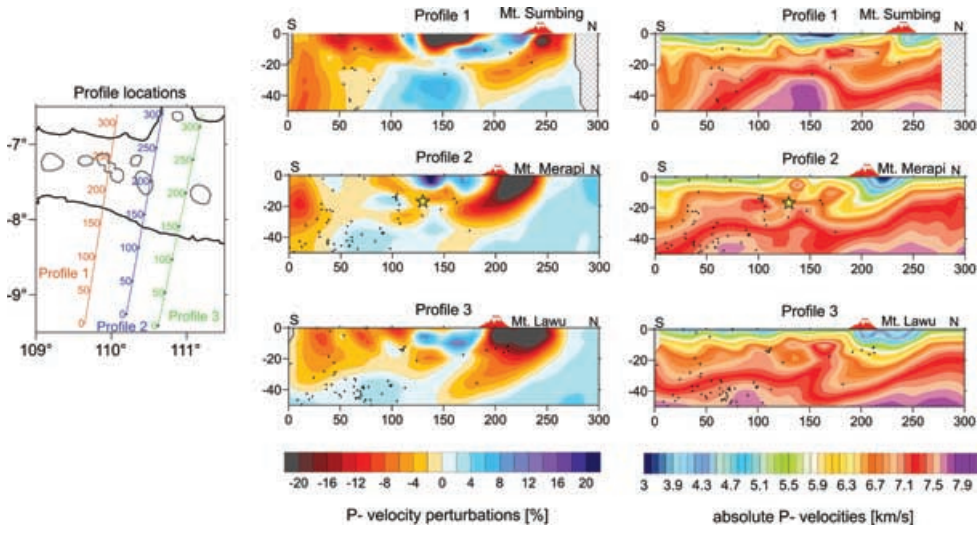

Figure 5. Result of the joint inversion for the *P*-velocity model presented in vertical sections. Profile locations are shown in the map on the left. The middle column presents relative perturbations of *P*-velocity; plots on the right show absolute velocities. Black dots mark hypocentres of the MERAMEX catalogue, the star in profile 2 marks the hypocentre of the Java earthquake in 2006 May.

seismicity and low-velocity anomaly is highest south of Merapi, Profile 2. The hypocentre of the Java earthquake (2006/05/26) is located in the transition zone of these anomalies. A more detailed description of the anomalies and their interpretation are given below in the 'Discussion and conclusions' section.

SYNTHETIC TESTS

Synthetic testing is one of the most important steps in any tomographic investigation to verify the results. The non-uniqueness of the results of any seismic tomography, especially of one with natural sources with unknown coordinates, requires that the model is validated carefully. The solution appears to be uncertain with regards to absolute amplitudes and the shape of anomalies. In addition, the trade-off between the velocity structure and source parameters has to be taken into account. The most difficult problem of tomographic analyses is to prove that the resulting images have some relevance to the structures in the real earth. In case of correct application, synthetic testing is able to provide reliable estimates for true amplitudes of the retrieved anomalies (Koulakov *et al.* 2007) to give us an idea about true resolution provided by the observation system and to separate true features from artefacts.

Our algorithm for synthetic modelling allows the definition of various synthetic models either as periodical anomalies in a checkerboard test or manually by drawing various shapes in vertical or horizontal sections. The traveltimes for the synthetic test are computed by 3-D ray tracing in a synthetic velocity model using real source–receiver pairs. In addition, random noise ϵ is added to the traveltimes. Usually, we define the shape of the noise according to a histogram of the residual distribution in the real data set. The synthetic times computed in this way are then used as input for the whole inversion procedure, including Step 1 (absolute source location) for the passive data. The values of all free parameters for the reconstruction of the synthetic model are the same as those used for the real data inversion.

To evaluate the resolving capabilities of the model in different parts of the study area, we performed a checkerboard test. The initial synthetic model was defined in the whole area as periodical anomalies of 30 km in size. The amplitude of velocity contrast was set to ± 7 per cent. In this test, we added 0.15 s rms random noise to the data set. The results of this test are presented in Fig. 6 separately for the active, passive and combined data sets for the depths of 5 and 15 km. For deeper sections, the resolution is controlled by passive data only, and the results are the same as those shown in Koulakov *et al.* (2007). Fig. 6 shows that the passive data cannot provide any resolution in the offshore part of the investigated area above 5 km depth. Adding the active data significantly extends the resolved area southwards and improves the accuracy and quality of the retrieved model, due mainly to the known positions of sources.

DISCUSSION AND CONCLUSIONS

The seismic reflection and refraction data acquired along the offshore profiles P16, P18 and P19 during RV Sonne cruise SO179 were forward modelled to obtain the *P* wave velocity field and trend of the main interfaces in the offshore area including the subduction zone. Three independent 2-D models of each seismic profile were developed and subsequently merged. It is possible to compare the offshore anomalies obtained by seismic tomography with the 2-D models of the forward modelling. The forward and tomography models show a high degree of correlation. In particular, the high-velocity anomaly in the west at the crossing point of profiles P18 and P19 (Figs 3 and 4) corresponds to a basement high, which can also be detected in the bathymetry data. It correlates with increased velocities in this area in the 2-D models of the two modelled seismic profiles. The anomaly vanishes at a depth of about 10 km, which is apparent in both tomographic and forward modelling results.

Thanks to the active 3-D data we were able to significantly improve the reliability of the tomographic models in the uppermost 20 km depth in the forearc region. In particular, the uppermost crust in the new model in the onshore part consists of two high-velocity blocks. The contact zone is marked by an elongated low-velocity zone of slightly oblique orientation with respect to the southern coast (Fig. 7). The epicentre of the Java earthquake (2006/05/26) is located just at the edge of this zone. We interpret this low-velocity zone as a weakened area between two rigid forearc blocks (see horizontal section showing the active data in Fig. 3). The decrease in velocity in this zone might be due to the fracturing of rocks

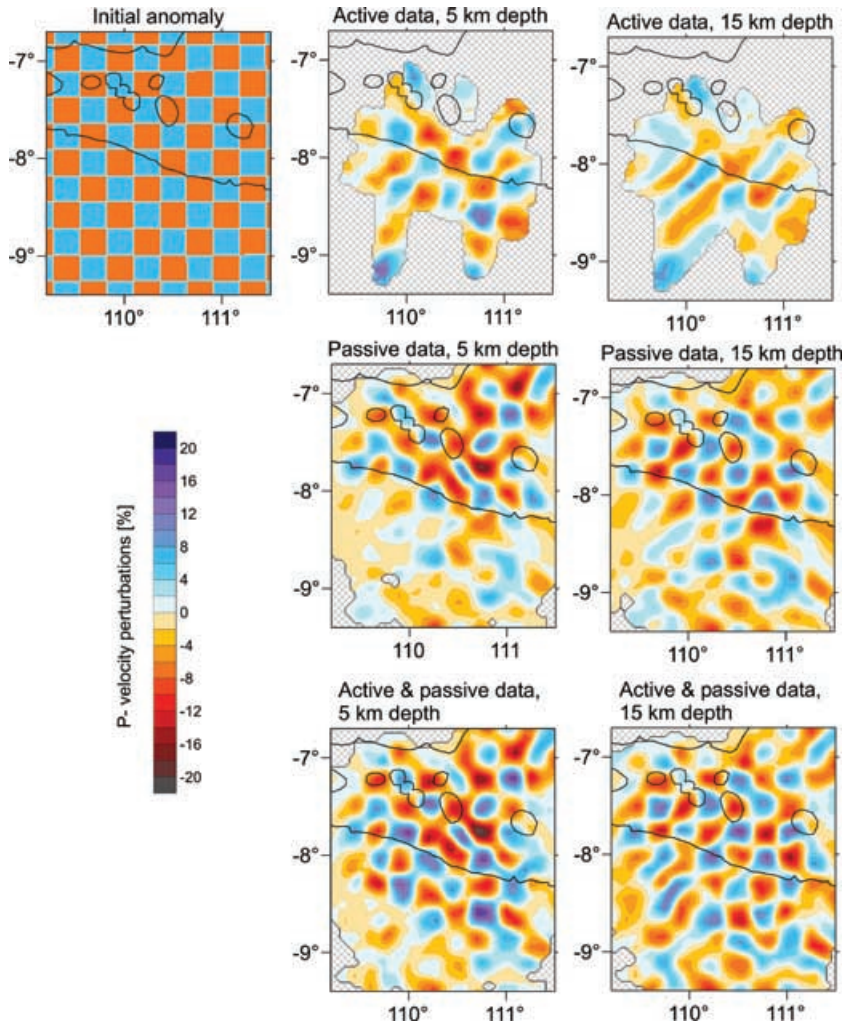

Figure 6. Comparison of the checkerboard tests for active, passive and combined data sets. The upper left image is the initial shape of anomalies with amplitudes of ±7 per cent. Noise of 0.15 s rms was added to the data in all cases. The 1st, 2nd and 3rd rows show results of reconstruction for the active, passive and combined data sets. Here, we present the results at two depths: 5 and 15 km.

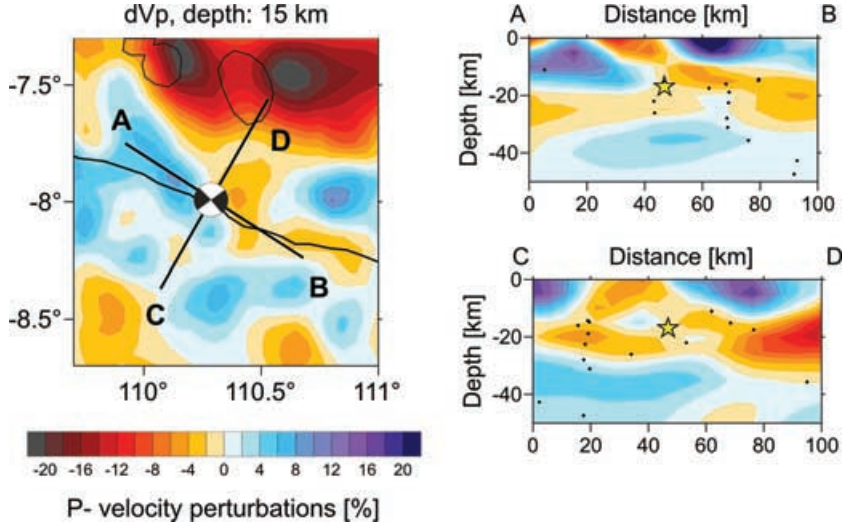

Figure 7. The left diagram shows a zoomed-in horizontal section of the joint inversion at 10 km depth. The two black lines indicate the positions of vertical sections crossing the BGR hypocentre of the Java earthquake in 2006 May. Black dots mark earthquake hypocentres of the MERAMEX catalogue.

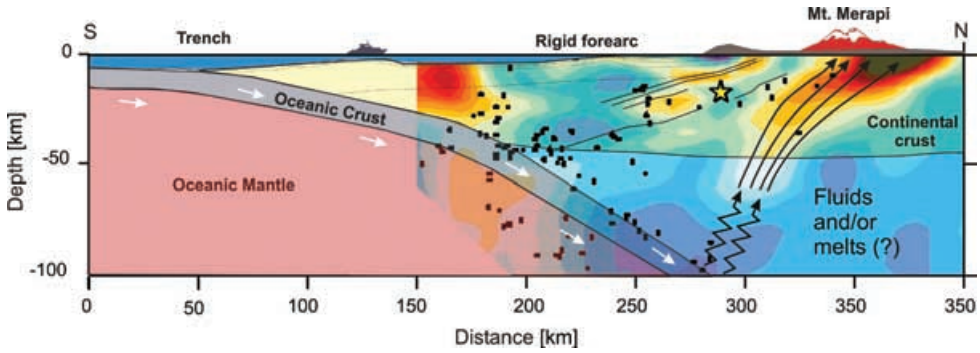

Figure 8. Sketch and interpretation of the velocity structure in Central Java. The oceanic plate pushes northward and subducts under Java. Partial melting occurs at a depth of about 100 km. Fluids and melts are ascending, thereby feeding the volcanoes located at the edge of the low-velocity anomaly. Stresses accumulate in the forearc region where fractures occur. Black dots show the earthquake distribution of the MERAMEX catalogue. The weakened low-velocity zone in the forearc correlates with the earthquake locations. The yellow star marks the BGR hypocentre of the Java earthquake in 2006 May.

in the uppermost crust. In the lower sections, at 15 km depth, this zone is almost invisible. The earthquake hypocentre is located just below this level (∼17 km depth). This implies that it is located in the rigid crust, just below the weakened zone, that is the most probable location for stress accumulation and rupture (see Fig. 8). The focal mechanism shows that the fault plane is oriented in the same direction as the weakened low-velocity zone. Fig. 7 shows a zoomed-in horizontal section of the joint inversion at 15 km depth and two vertical cross sections through the earthquake epicentre. The epicentre in the vertical section CD (Fig. 7) falls into a high-velocity layer, which is located just above the inclined contact zone between the high-velocity forearc and the low-velocity anomaly (MLA) northward of the volcanoes. The vertical section AB shows the epicentre well above the low-velocity anomaly.

We tentatively present an explanation for the origin of seismicity in the forearc on a larger scale in Fig. 8. The distribution of the seismicity in the Benioff zone indicates a variable dipping angle of the slab. For the first 150 km from the trench, the slab appears to be almost horizontal and then the dipping angle increases rather sharply to 45°. This change might cause a northward pushing and stress accumulation in the overriding plate. The observed local seismicity in the forearc including the Java event of 2006 May 26 can be due to this mechanism. The inclined linear anomalies in the forearc might reflect the distribution of weakened fracture zones, which are also observed in the active OBH data. The model in Fig. 8 also relates the active volcanism in Central Java to the subduction processes. Earthquakes in the Benioff zone at a depth of about 100 km are related to a phase transition in the slab causing fluid release and partial melting of the oceanic crust. The melting temperature in the mantle wedge is reduced by the ascending fluids. Above 60 km depth an inclined low-velocity anomaly can be detected in the tomographic sections and it may be attributed to partial melting. The ascending fluids rise further upwards, get blocked by the rigid tectonic bodies of the forearc and move on northwards along the bottom of the forearc (see Fig. 8). After the ascending fluids and melts have reached the northern boundary of the forearc, they form high concentrations of gases and magma and cause active volcanism.

Smyth *et al.* (2005) divide eastern Java into four east–west oriented zones (1) the southern Mountain zone, (2) the present-day volcanic arc, (3) the Kendeng zone and (4) the Rembang zone. The Kendeng zone represents a basin, which extends about 400 km in the east–west and about 100–120 km in the north–south direction and contains more than 8 km of sediments (Untung and Sato 1978; Smyth *et al.* 2005). Bouguer gravity maps of Central Java (Untung & Sato 1978; Smith & Sandwell 1997; Smyth *et al.* 2005) show a strong negative Bouguer anomaly located in this zone, exceeding $-580\ \mu\ \mathrm{ms}^{-2}$. The gravity low presents a high correlation in size and location with the low-velocity anomaly MLA discussed above. While previous studies interpreted the basin as a rift, Smyth *et al.* (2005) propose no crustal thinning. They suggest that flexural loading of the crust by the volcanic chain contributed to the subsidence in this region. Waltham *et al.* (2006) forward modelled the gravity data. They needed a high density volcanic arc to model the gravity low accurately and propose that there are additional buried loads, which could be due to magmatic underplating.

The MLA has its maximum amplitude of over 30 per cent at 5 km depth and decreases with depth (see Figs 4 and 5). Hence, the exceptionally high amplitudes of the low-velocity anomaly in the uppermost 10 km is related to and partly caused by thick lava and sedimentary deposits in the Kendeng zone. But these deposits cannot explain why the MLA can also be detected in deeper depth sections and even in the mantle. In addition, these deposits alone cannot prevent magma penetrating to the surface and cannot explain the gravity anomaly completely. For the fact that we do not observe any volcanism above the MLA and the additional loads for the gravity modelling a possible explanation was suggested in a personal communication with V. Troll (2006). It was proposed that the material in the MLA is actually at a stage of cooling, which resulted in producing a rigid matrix filled with pockets of molten materials. As a result, this zone should be fairly rigid and of low-velocity. Thus, the fluids and melts from the mantle wedge cannot pass through and follow the bottom boundary of the MLA. The fluids and melts follow the shortest way towards the contact zone between the MLA and the forearc, where the active volcanoes are located. Only small amounts of fluids, which form mud volcanoes in the Kendeng zone pass through the matrix of sedimentary deposits and magma pockets.

In the future, we will work on the gravity data acquired during RV Sonne cruise 179 and model these data along the seismic profiles. These models will be compared with the seismic and tomographic models. Having done so, velocity models covering Central Java up to the Java trench can be constructed and a composite model of the subduction zone and its linkage to the volcanic source of Merapi volcano will be available. The MLA will be further investigated by studies regarding anisotropy and attenuation. Additional tomographic studies will focus on 2-D models of the seismic profiles P16

and P18, resulting in images of the velocity distribution reaching from close to the south coast of Central Java over the Java trench. We also plan to perform tomography analyses to determine anisotropic properties of the crust and the upper mantle, which seem to have a crucial influence on the geophysical characteristics of Central Java. Significant improvement of the structure around the epicentre of the Java earthquake (2006/05/26) will be achieved based on the information on the aftershocks presently recorded by a temporary network consisting of 12 stations installed by GFZ in Central Java.

ACKNOWLEDGMENTS

This is publication no. GEOTECH-251 of the R&D Programme GEOTECHNOLOGIEN funded by the German Ministry of Education and Research (BMBF), the German Research Foundation (DFG), Grant 03G0579C and the GeoForschungsZentrum Potsdam (GFZ). Detailed and constructive reviews and editorial remarks by G. Laske, S. Gregersen and one anonymous reviewer are greatly appreciated. Essential support of the project was provided by the Center for Volcanology and Geological Hazard Mitigation (CVGHM) Bandung, the Volcanological Technology Research Center (BPPTK) Yogyakarta, the Gadjah Mada University (UGM) Yogyakarta, Institut Teknologi Bandung (ITB) Bandung and the Meteorological and Geophysical Agency (BMG) Jakarta. The geophysical data offshore were acquired using RV SONNE as platform. We are grateful to Cpts. Papenhagen and Mallon and their crews for their professional work at sea. We would like to thank all Indonesian and German partners and participants of the fieldwork. The instruments were provided by the Geophysical Instrument Pool Potsdam (GIPP), the Christian Albrecht University, Kiel, and the IFM-GEOMAR, Kiel. Many thanks also to V. Troll and his colleague for the helpful discussions.

REFERENCE

Beauducel, F. & Cornet, F.H., 1999. Collection and three-dimensional modeling of GPS and tilt data at Merapi volcano, Java, *J. Geophys. Res.*, **104**(B1), 725–736.

Berthommier, P.C., 1990. Étude volcanologique du Merapi (Centre-Java), Téphrostratigraphie et chronologie—produits éruptifs, Thèse Doct., Université Blaise Pascal, Clermont-Ferrand, France, pp. 115.

Camus, G.A., Gourgaud, P.-C., Mossand-Berthommier, P.-C. & Vincent, P.M., 2000. Merapi (Central Java, Indonesia): an outline of the structural and magmatological evolution, with a special emphasis to the major pyroclastic events. *J. Volcanol. Geother. Res.*, **100,** 139–163.

Hamilton, W., 1988. Plate tectonics and island arcs, *Geol. Soc. Am. Bull.,* **100,** 1503–1527.

International Seismological Centre, 2001. Bulletin Disks 1–9 [CD-ROM], Internatl. Seis. Cent., Thatcham, United Kingdom.

Kennett, B.L.N. & Cummins, P.R., 2005. The relationship of the seismic source and subduction zone structure for the 2004 December 26 Sumatra-Andaman earthquake, EPSL 239, pp. 1–8.

Kennett, B.L.N., Engdahl, E.R. & Buland, R., 1995. Constraints on seismic velocities in the Earth from traveltimes, *Geophys. J. Int.,* **122,** 108–124.

Kopp, H., Flueh, E.R., Petersen, C.J., Weinrebe, W., Wittwer, A. & Meramex Scientists, 2005. The Java margin revisited: evidence for subduction erosion off Java, *Earth planet. Sci. Lett.,* **242,** 130–142.

Koulakov, I., Sobolev, S.V. & Asch, G., 2006a. P- and S-velocity images of the lithosphere-asthenosphere system in the Central Andes from local-source tomographic inversion, *Geophys. J. Int.,* **167,** 106–126.

Koulakov, I. & Sobolev, S., 2006b. Moho depth and three-dimensional P and S structure of the crust and uppermost mantle in the Eastern Mediterranean and Middle East derived from tomographic inversion of local ISC data, *Geophys. J. Int.,* **164**(1), 218.

Koulakov, I. *et al.*, 2007. P- and S-velocity structure of the crust and the upper mantle beneath Central Java from local tomography inversion, *J. Geophys. Res.,* submitted.

Maercklin, N., Riedel, C., Rabbel, W., Wegler, U., Lühr, B.-G. & Zschau, J., 2000. Structural investigation of Mt. Merapi by an active seismic experiment, in *Deutsche Geophys,* IV/2000, pp. 13–16, Gesellschaft-Mitteilungen, Sonderband.

Masson, D. G., 1991. Fault patterns at outer trench walls, *Mar. Geophys. Res.,* **13,** 209–225.

Mignan, A., King, G., Bowman, D., Lacassin, R. & Dmowska, R., 2006. Seismic activity in the Sumatra-Java region prior to the December 26, 2004 (Mw = 9.0–9.3) and March 28, 2005 (Mw = 8.7) earthquakes, *EPSL,* **244,** 639–654.

Moore, G. F., Curray, J.R., Moore, D.G. & Karig, D.E., 1980. Variations in geologic structure along the Sunda Fore Arc, Northestern Indian Ocean, in *The Tectonic and Geological Evolution of Southeast Asian Seas and Islands*, pp. 145–160, ed. D.E. Hays, Geoph. Mon. 23,.

Müller, A. & Haak, V., 2004. 3-D modeling of the deep electrical conductivity of Merapi volcano (Central Java): integrating magnetotellurics, intuction vectors and the effects of steep topography, *J. Volcanol. Geother. Res.,* **138,** 205–222.

Müller, M., Hördt, A. & Neubauer, F.M, 2002. Internal structure of Mount Merapi, Indonesia, derived from long-offset transient electromagnetic data, *J. Geophys. Res.,* **107**(B9), 2187.

Newhall, C.G., Bronto, S., Alloway, B., Banks, N.G., Bahar, I. & Marmol, M.A.D., 2000. 10000 Years of explosive eruptions of Merapi volcano, Central Java: archaeological and Modern Implications, *J. Volcanol. Geother. Res.*, **100,** 9–50.

Ratdomopurbo, A. & Poupinet, G., 2000. An overview of the seismicity of Merapi volcano (Java, Indonesia), 1983 – 1994. *J. Volcanol. Geother. Res.,* **100,** 193–214.

Smith, W.H.F. & Sandwell, D.T., 1997. Global seafloor topography from satellite altimetry and ship depth soundings, *Science,* **277,** 1957–1962.

Smyth, H.R., Hall, R., Hamilton, J. & Kinny, P., 2005. East Java: Cenozoic Basins, Volcanoes and Ancient Basement, *Proceedings, Indonesian Petrolium Association*, Thiertieth Annual Convention & Exhibition.

Tiede, C., Camacho, A.G., Gerstenecker, C. & Fernández, J., 2005. Modelling the density at Merapi volcano area, Indonesia, via the inverse gravimetric problem, *Geochem., Geophys., Geosys. (G3),* **6**(9), 1–13.

Tregoning, P. *et al.*, 1994. First geodetic measurement of convergence across the Java Trench, *Geophys. Res. Lett.,* **21**(19), 2135–2138.

Um, J. & Thurber, C., 1987. A fast algorithm for two-point seismic ray tracing, *Bull. Seism. Soc. Am.,* **77,** 972–986.

Untung, M., & Sato, Y., 1978. Gravity and geological studies in Java, *Indonesia: Geological Survey of Indonesia and Geological Survey of Japan,* Special Publication, 6, 207 pp.

Waltham, D., Hall, R. & Smyth, H.R., 2006. Basin formation by volcanic-arc loading. *GSA Special Paper: formation and applications of the sedimentary record in arc collision zones (ed A Draut),* in press.

Wegler, U. & Lühr, B.-G., 2001. Scattering behavior at Merapi volcano (Java) revealed from an active seismic experiment. *Geophys. J. Int.,* **145,** 579–592.

Wittwer, A., Kopp, H., Wagner, D., Flueh, E.R. & Rabbel, W., 2007. Crustal and upper mantle structure of the central Java subduction zone from marine wide-angle seismics, in preparation.